Automatic Extraction of the Structure of the Retinal Blood Vessel Network of Premature Infants

Lassada Sukkaew MSc*,
Bunyarit Uyyanonvara PhD*, Sarah Barman PhD**,
Alistair Fielder MD***, Ken Cocker MD***

* Sirindhorn International Institute of Technology, Thammasat University, Thailand
** Kingston University, United Kingdom
*** City University, United Kingdom

Objective: *Automatically detect the structure of blood vessels in ROP infants to allow ophthalmologist to analyze and detect the symptom early.*

Material and Method: *This study presents a set of methods for detection of the skeletonized structure of premature infant's low-contrast retinal blood vessel network. Steps has been optimized for this study, namely statistically optimized LOG edge detection filter, Otsu thresholding, Medial Axis transform skeletonization, pruning, and edge thinning.*

Results: *A set of 100 test images are grouped together into five testing groups based on their similar characteristics and clinicians suggestions. The authors applied the series of methods proposed on all the 100 images. The result from the algorithm was compared with ophthalmologists' hand-drawn ground truth and it can detect the blood vessel with a high specificity of 0.9879 and sensitivity of 0.8935.*

Conclusion: *The authors' algorithm can detect blood vessels effectively even though the image quality may not be good, have high noise, and low contrast. The algorithm can also detect the blood vessel at important locations such as the edge of the retina.*

Keywords: *Retinal vessel extraction, ROP, Infant retinal image*

Retinopathy of Prematurity (ROP) is an abnormal retinal vascularization in premature infants. In those infants, the growth of retinal vessels does not reach the periphery of the retina. Generally, the development of retinal vessel network begins to grow at approximately 15 weeks of gestation from the optic disk into the retina and becomes complete around full term at 9 months. Preterm birth carries many complications because this vessel is not fully vascularized. The early indicator of ROP is a whitish gray demarcation line between the normal retina and the anteriorly undeveloped vascularized retina. Next, there will be ridge that obstructs vascular growth and causes congestion of capillaries around the periphery of retina. As the condition progresses, extraretinal fibrovascular pro-liferations develops. If left untreated, it may cause retinal traction and the loss of vision. The important risk factors for ROP are low birth weight and low gestational age. To prevent permanent loss of vision, infants at risk with less than 1,500 gram birth weight or less than 32 week gestational ages should be screened for ROP to receive appropriate treatment (UK guidelines - there are differences between countries)[1]. Several researchers have attempted to establish techniques for initial diagnosis of vascular abnormalities. They developed an automatic vascular inspection system to analyze physical characteristics and abnormalities of vessels by measuring size, shape, and length or network characteristics of the retina. This development of algorithms to automatically provide classification of vessels usually gives a satisfactory result in a high quality image with low noise. However, due to the lack of clarity of the eye media and the technical difficulty

Correspondence to : Sukkaew L, Sirindhorn International Institute of Technology, Thammasat University, Pathumthani 12000, Thailand.

of obtaining images from a preterm baby, images taken from a baby's eye are low-contrast, noisy, and sometimes blurred. These cause problems and are an obstacle to the classification of vessels. Algorithms that have been successfully applied for adult retinal images might not work effectively enough within these limitations. A challenging problem to investigate disease and symptoms of ROP is the requirement to detect the vascular network in the retina. This information can then be used for the measurement of tortuosity and engorgement parameters.

Many works have been proposed to detect ROP signs effectively by visual inspection of retinal blood vessels. The main vessel properties indicating ROP are an increase in vessel width and tortuosity[2-5]. Regular inspection produces a large number of retinal photographs for ophthalmologists and experts to review. This might be cut down by the use of digital imaging technology that provides means for non-ophthalmologists to automate the preliminary diagnosis of the disease[6]. Many papers such as Martinex-Perez et al[7] reported a semi-automatic method to measure and quantify the geometrical and topological properties of retinal blood vessel from fundus retinal images. Chanwimaluang and Fan[8] and Gao et al[9] introduced efficient methods for automatic detection and extraction of blood vessels. Canny experimented with an algorithm of matched filters[10] for vessel detection. Chaudhuri[11] used a Gaussian vessel cross-sectional profile and assumed Gaussian imaging noise for vessel detection using matched filters. A method of registration of retinal images based on feature detection was reported by Byrne et al[12]. Line finding algorithms along with a probabilistic relaxation scheme has been proposed to extract and describe the blood vessel pattern in retinal images by Akita[13-15]. These segments were later connected to a vessel network and labeled as arteries or veins according to their chromatic information. Tolias and Panas[16] developed a fuzzy C-means (FCM) clustering algorithm that uses linguistic descriptions like "vessel" and "nonvessel" to track fundus vessels in retinal angiogram images. Quek[17], Hoover[18], Chutatape[19] and Zhou[20], proposed similar methods based on a matched filter to extract vasculature from two dimensional medical images. Gang et al[21] showed the Gaussian curve is suitable for modeling the intensity profile of the cross section of retinal vessels in color fundus images. Aylward[22] extracted blood vessels from two-dimensional images using a scale space technique with sub-voxel accuracy while Wood[23] equalized image variability as a preprocessing step in their method to

segment retinal vessels. Neural network application is proposed by Sinthanayothin et al[24]. It employed intensity edge detection and principal component analysis of input images as inputs to multilayer perceptron neural networks to identify blood vessels. Nekovei and Sun[25] detected blood vessels in XRA images using a back-propagation network. Leandro et al[26] used a continuous wavelet transform combined with morphological operators to segment blood vessels within the retina. Staal[27] presented a method to detect vessels by proposing a more natural representation for elongated structures, such as vessels. Parvin et al[28], Huang and Stockman[29], and Aylward et al[30] described similar algorithms that used generalized cylinders to extract tubular structures in 2D intensity images. Mahadevan et al[31] presented a set of algorithms for robust detection of vasculature in noisy retinal video images. Gao et al[32] presented an automatic quantification of blood vessel topography in retinal images. This system utilized digital image processing techniques to provide more reliable and comprehensive information for the retinal vascular network. Vermeer et al[33] proposed a method for blood vessel detection in retinal images based on a Laplace and threshold segmentation. Ayala et al[34] presented a main idea to define the averages of a given fuzzy set by using different definitions of the mean of a random compact set of retinal vessel detection.

Many previous techniques have demonstrated that they can be applied successfully on adult images. However, those methods are not sufficient to detect vessels on infant images. There are many differences between the adult and infant image such as visibility of the blood vessels, global noise in the image, and thickness of vessels. Fig. 1 shows (a) an example of an infant retinal image and (b) an example image of an adult retinal image. However, retinal blood vessel detection in infants is equally important as detection of blood vessels in adults even though it is a more difficult problem.

Material and Method

The authors have experimented with the application of many adult images algorithms on infant retinal images taken using a RetCam120 camera. A successful combination of those statistically optimized algorithms for the infant retinal vessels classification is explained in this section.

Statistically optimized Laplacian of Gaussian filter for infant's low-contrast image edge detection

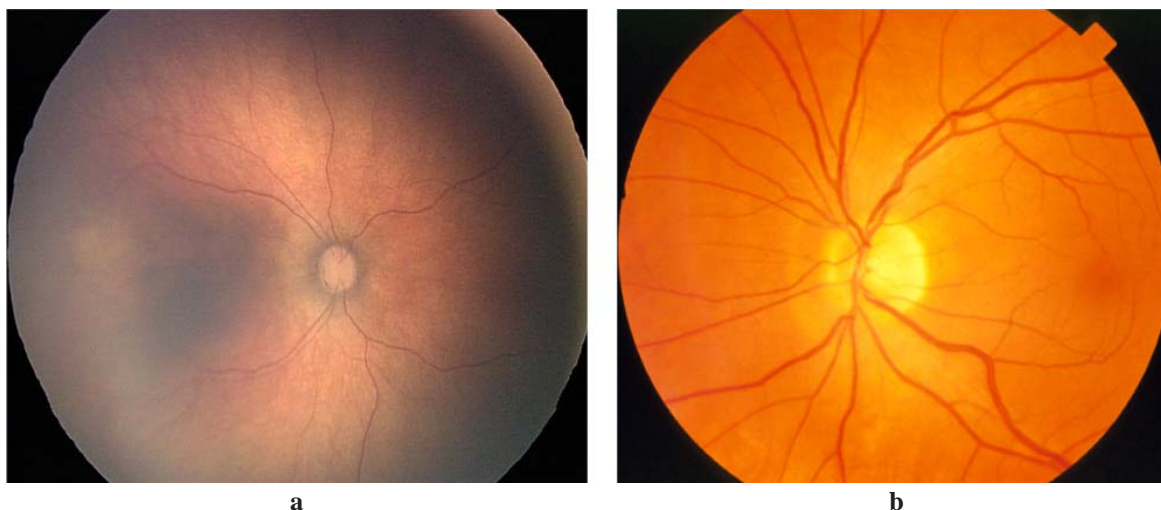The edges in an image give structural infor-

Fig. 1 (a) Example image of an infant retina
  (b) Example image of an adult retina

mation about its boundaries. To detect blood vessels, edge information is significantly important because the vessels are clearly visible in an edge image. The authors' first step was to extract edge information from the original infant retinal image. After qualitative comparison of the performances between many public domain edge operators with the set of infant images, the authors found that Laplacian of Gaussian (LOG) detected blood vessel from most of the data set very well. The LOG operator is described by equation (1)[40].

$$LOG(x, y) = \frac{-1}{2\pi\sigma^4}\left[2 - \frac{x^2 + y^2}{\sigma^2}\right]e^{-\frac{1}{2}\left(\frac{x^2+y^2}{\sigma^2}\right)} \quad ....(1)$$

where (x,y) is the size of optimal kernel filter and the scale parameter σ is estimated adaptively between 1.0-1.6.

However, a few parameters needed to be optimized to reflect the infant retinal image. An effective result depends on the right size of an optimal kernel filter. Statistical variation of σ and operator size was then investigated. The authors varied σ from 1.0 to 1.6 in 0.1 steps. Operator size was also experimented from 3 x 3, 5 x 5, 7 x 7, and up to 21x21 because the actual size of blood vessel was unknown at the beginning. All the combinations of σ and operator size were then applied on a test set of 20 images. Fig. 2 and 3 show some chosen results after variation of σ and operator size.

Statistically, the authors found that an σ of 1.4 at the operator size of 11 x 11 yielded the best performance[35-36].

Medial Axis Skeletonization

The skeletonized structure is useful information because it provides a simple and compact representation of a shape and preserves many of the topological and size characteristics of the original shape at the same time. The length of a shape can be calculated by considering just the end points of the skeleton and finding the maximally separated pair of end points on the skeleton. It is crucial that the authors can find underlying structure of the vessel automatically because many ophthalmologists consider the abnormality of the retina by looking at the orientation and complexity of blood vessel structure[37-38]. The edge image from the previous step will be at threshold and skeletonized in this section. Before the resulting edge image from the previous step is skeletonized with Medial Axis Skeletonization algorithm, Otsu's thresholding algorithm was applied to binarise the image into two classes, black and white. Otsu method automatically chooses the threshold to minimize the intraclass variance of the black and white pixels[39].

The Medial Axis Skeletonization algorithm is chosen from quantitative experiments and applied to the binary image in this step in order to extract structure of the blood vessels. The vessel tree is then created by connecting these centerlines Medial Axis Transform is defined as the locus of the centre of all the maximal inscribed circle of the object as described in equation (3).

The medial axis transform of an image *A* is determined by the medial axis of *A* and the medial axis
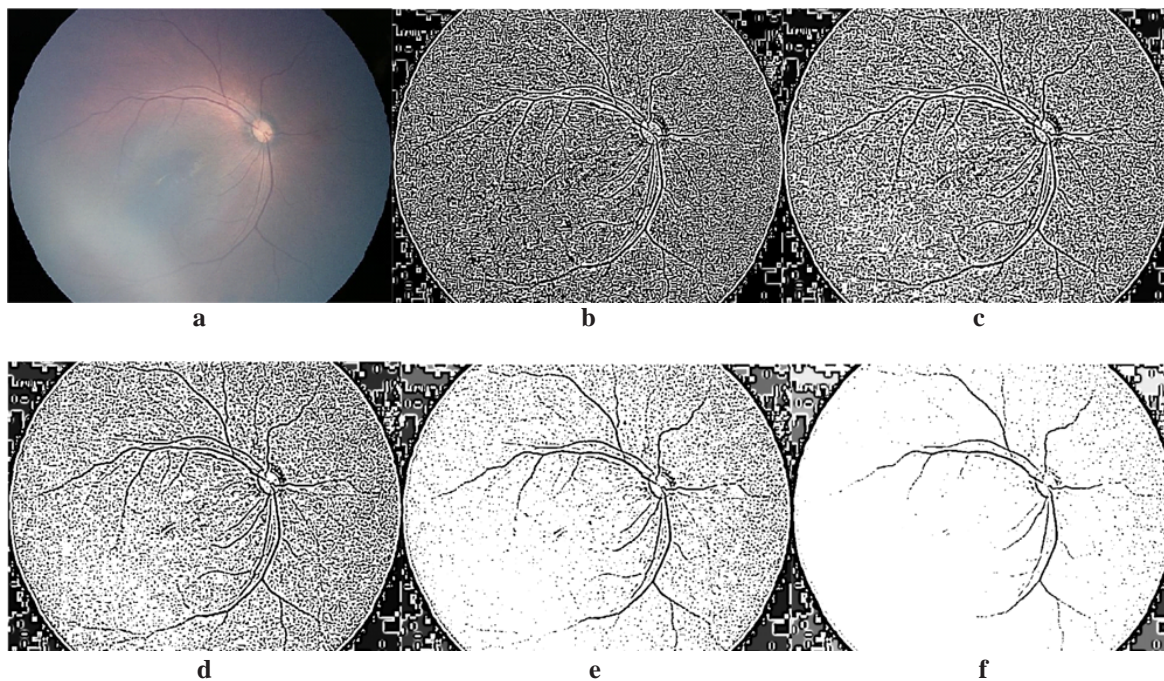
Fig. 2   (a) original image and (b), (c), (d), (e), (f) are resulting images after application of fixed operator size 11 x 11 and σ is varied 1.2, 1.3, 1.4, 1.5 and 1.6 respectively
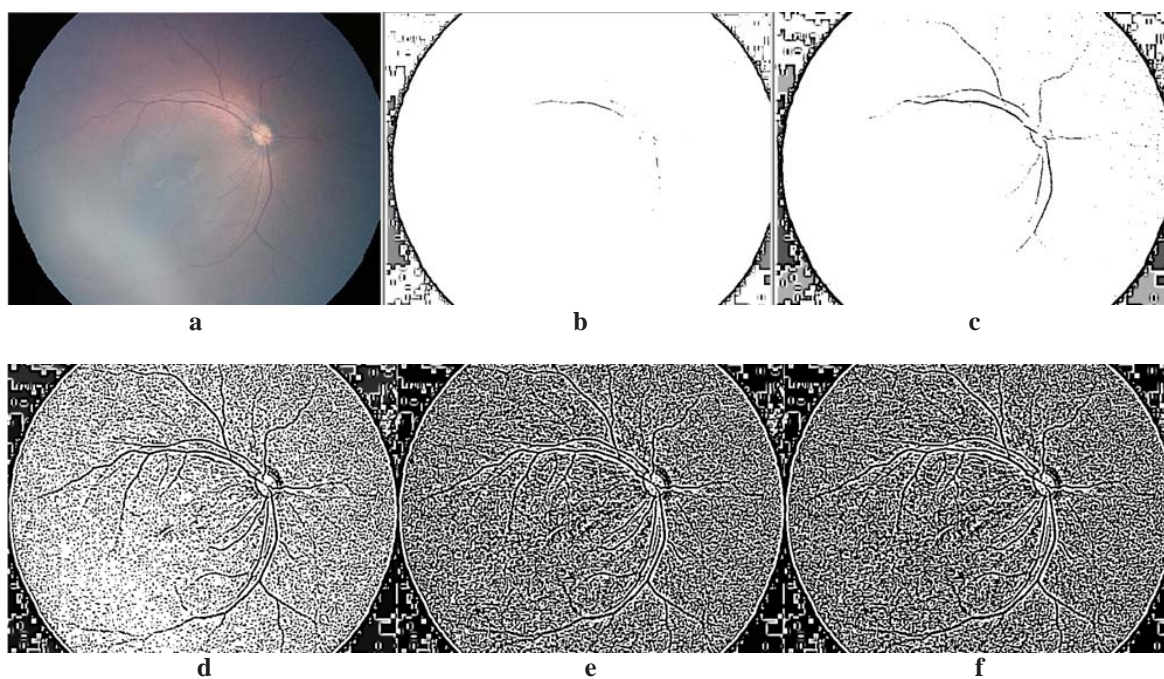

Fig. 3   (a) original image and (b), (c), (d), (e), (f) are resulting images after application of fixed σ and varied operator size of 5 x 5, 9 x 9, 11 x 11, 13 x 13 and 15 x 15 respectively

distance function f defined on the medial axis of A. The medial axis function is directly related to the generalized distance. For the following definition of the morphological skeleton of an image A with respect to a structuring element K by the sets $\{S_0,..,S_N\}^{(40)}$ where,

$$S_n = A \ominus K - (A \ominus K) \circ K \text{ and } A \ominus K = A \quad ...(2)$$
$$ n n \phantom{\circ K \text{ and } A \ominus K} 0$$

The skeleton of an image A is then given by

$$S(A) = \overset{N}{\underset{n=0}{U}} S_n \quad ....(3)$$

($\ominus$ denotes erosion operator with n iterations and is $\circ$ an opening operator)

After the algorithm is applied, the blood vessels (including other artifacts) are thinner and can be visibly observed. In fact, it is only one pixel wide throughout the image except on the intersection points. The resulting skeleton is located at the central line of the original image. This result shows that the skeletonized image can clearly maintain the blood vessel topology and the blood vessel network as illustrated in Fig. 4. This valuable information is important when the authors later calculate other properties, like tortuosity of the blood vessel.

Image Pruning

The authors used of a series of morphological operations to reduce the size of the noise that is smaller than a specific size. One set of the series, known as image pruning, is used in this step. The resulting image from the previous step is processed with image pruning as defined by steps from equation (4) to equation (7).

$$X_1 = A \otimes \{B\} \quad ....(4)$$

$$X_2 = \overset{n}{\underset{k=1}{U}} (X_1 \circledast B^k) \quad ....(5)$$

$$X_3 = (X_2 \oplus H) \cap A \quad ....(6)$$

$$X_4 = X_1 \cup X_3 \quad ....(7)$$

where X_4 is the result of pruning set A with structuring element B [(41)]. X_1, X_2, and X_3 are resulting images of the intermediate process. $\otimes$ denotes a morphological thinning operator while $\oplus$ is a dilation operator. $\circledast$ denotes hit or miss transform. Three examples of results from this step are demonstrated in Fig. 5. Original images 5(a), 5(c), and 5(e) are processed and Fig. 5(b), 5(d), and 5(f) are their results respectively.
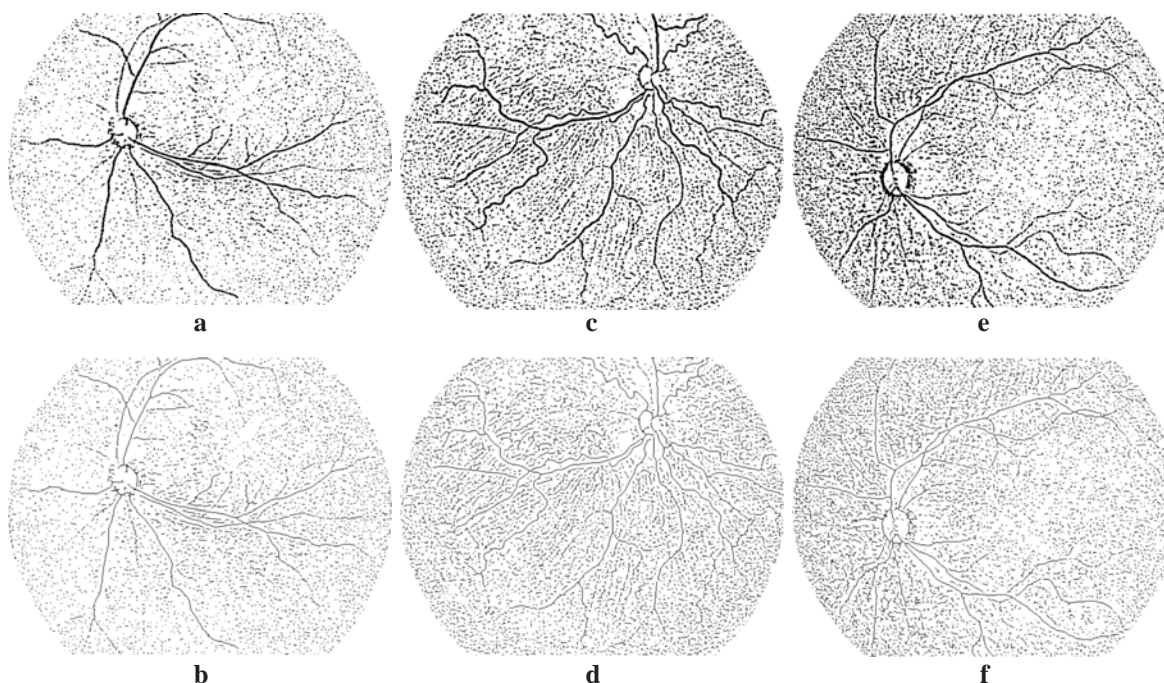

Fig. 4 Images on the right hand side (b), (d) and (f) are results of skeletonized process of images on the left hand side (a), (c) and (e) respectively
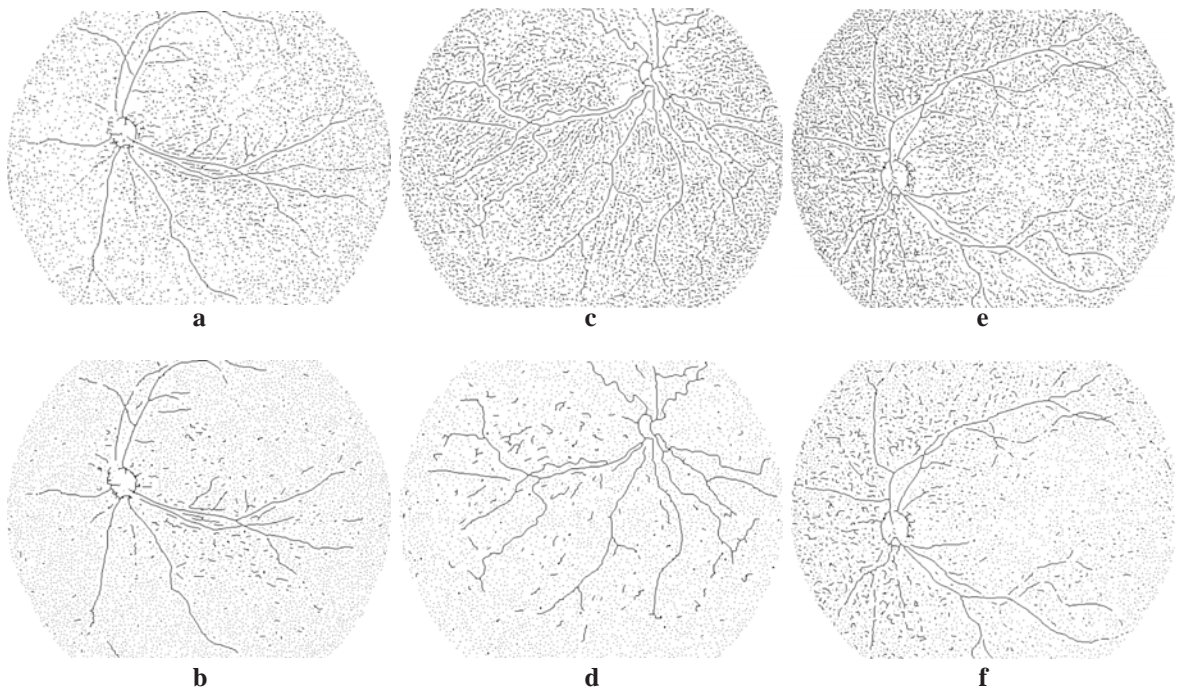
Fig. 5 Images on the right hand side (b), (d) and (f) are results of pruning process of images on the left hand side (a), (c) and (e) respectively
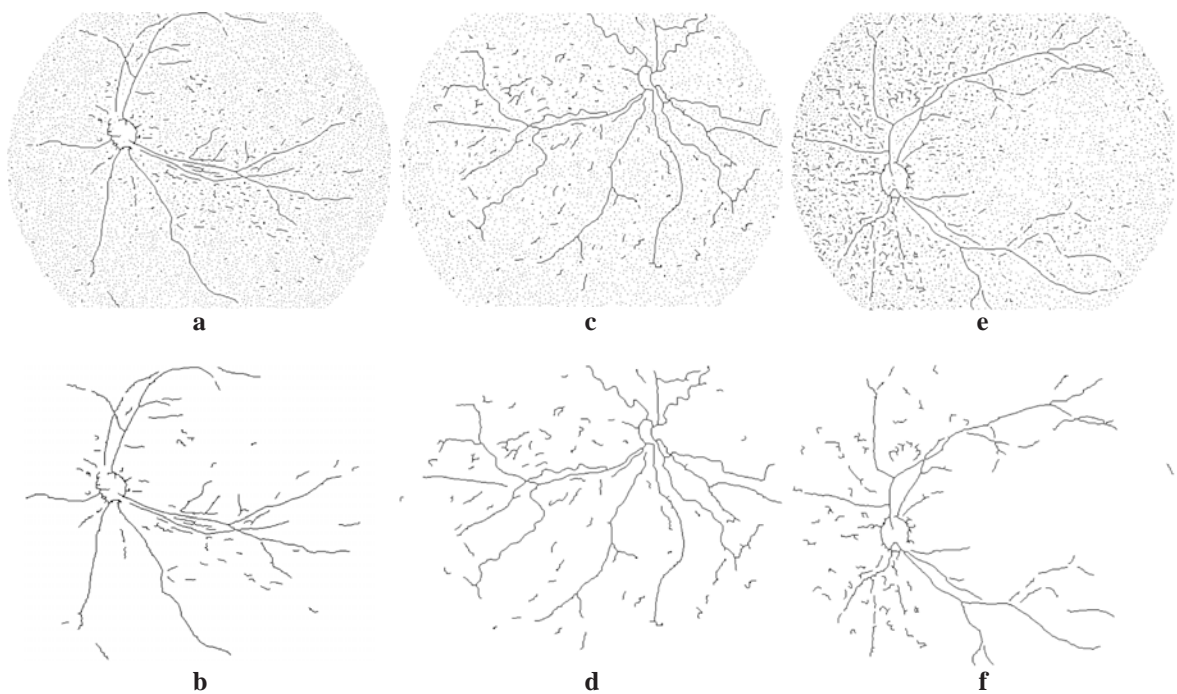

Fig. 6 Images on the right hand side (b), (d) and (f) are results of spur removal process of images on the left hand side (a), (c) and (e) respectively

Spur Removal by morphological Opening

The authors' last step in the process is to remove isolated noise, or spurs, a cluster of pixels that has a size less than 15 pixels. Morphological opening is chosen to use in this step because it is robust, fast and easy to implement. This island removal algorithm utilizes Erosion ($\ominus$) and Dilation ($\oplus$) (erosion followed by dilation) as in the following equation.

$$S = A \circ B = (A \ominus B) \oplus B \quad ....(8)$$

where S is the result after spur removal. Fig. 6 illustrates results from this step.

All of the authors' process described above can be summarized with a flowchart diagram in Fig. 7.

Fig. 8 shows the results from each step. Fig. 8(a) is an original infant retinal image. 8(b) is the result after the edge detection process. 8(c) is result after Otsu thresholding and 8(d) is the output after the authors applied Medial axis skeletonization. The result of the image pruning step is shown in 8(e) while 8(f) shows the result after Spur Removal. Fig. 8(g) is the skeletonized image superimposed on the original image to enhance blood vessel visibility.

Results

A set of 100 test images are grouped together into five testing groups based on their similar characteristics and clinicians suggestions, namely group A, B, C, D, and E. Group A contains images with fairly clear vessels while vessels in images in group B are difficult to distinguish. In group C, vessels of images in this set are very convoluted while the vessels in images in group D are less convoluted. Images in group E are very noisy or blurred. Examples of images in each test group are shown in Fig. 9.

The authors applied the series of methods proposed on all the 100 images and some of the results are shown in Fig. 10.

Discussion

To measure the performance of our method, the authors created ground truth images manually by drawing lines on vessel of original images. This is under supervision of a trained clinician. These 100 hand-drawn ground truth images are essential for performing a quantitative analysis of an algorithm's results. Both the ground-truth images and final result images are binary images, so they can be compared easily by using Exclusive-Or function. Some examples of ground truth images are shown in Fig. 11.
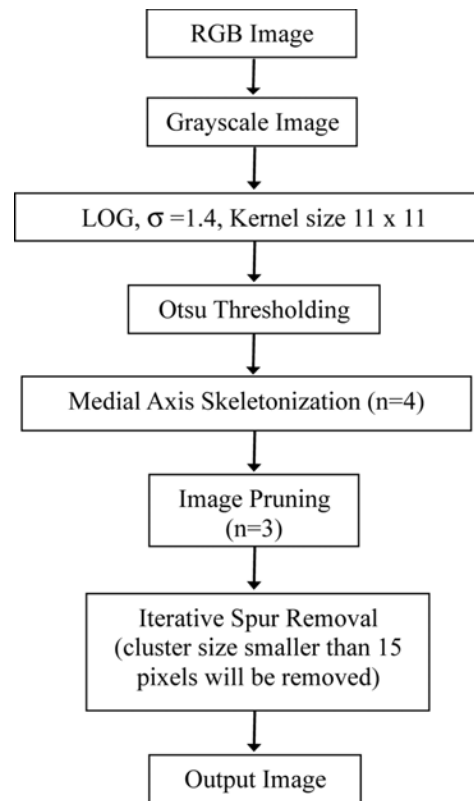

Fig. 7 Flowchart of the authors' proposed series of process to extract blood vessels' skeleton

The authors can calculate four different values from the comparison, namely, true positives (TP) or a number of pixels correctly detected as vessel pixels, false positives (FP) or a number of pixels incorrectly flagged, true negatives (TN) or a number of pixels correctly detected as non-vessel and, finally, false negatives (FN) or number of pixels incorrectly flagged as non-vessels. Fig. 12 graphically demonstrates the calculation.

The authors then used the 4 values from previous calculation to calculate performance measurement values, sensitivity (Se) and specificity (Sp) as follows

$$Se = \frac{TP}{TP + TN} \quad ....(9)$$

$$Sp = \frac{FN}{FN + FP} \quad ....(10)$$

Where TP is true positives, FP is false positives, TN is true negatives, and FN is false negatives.
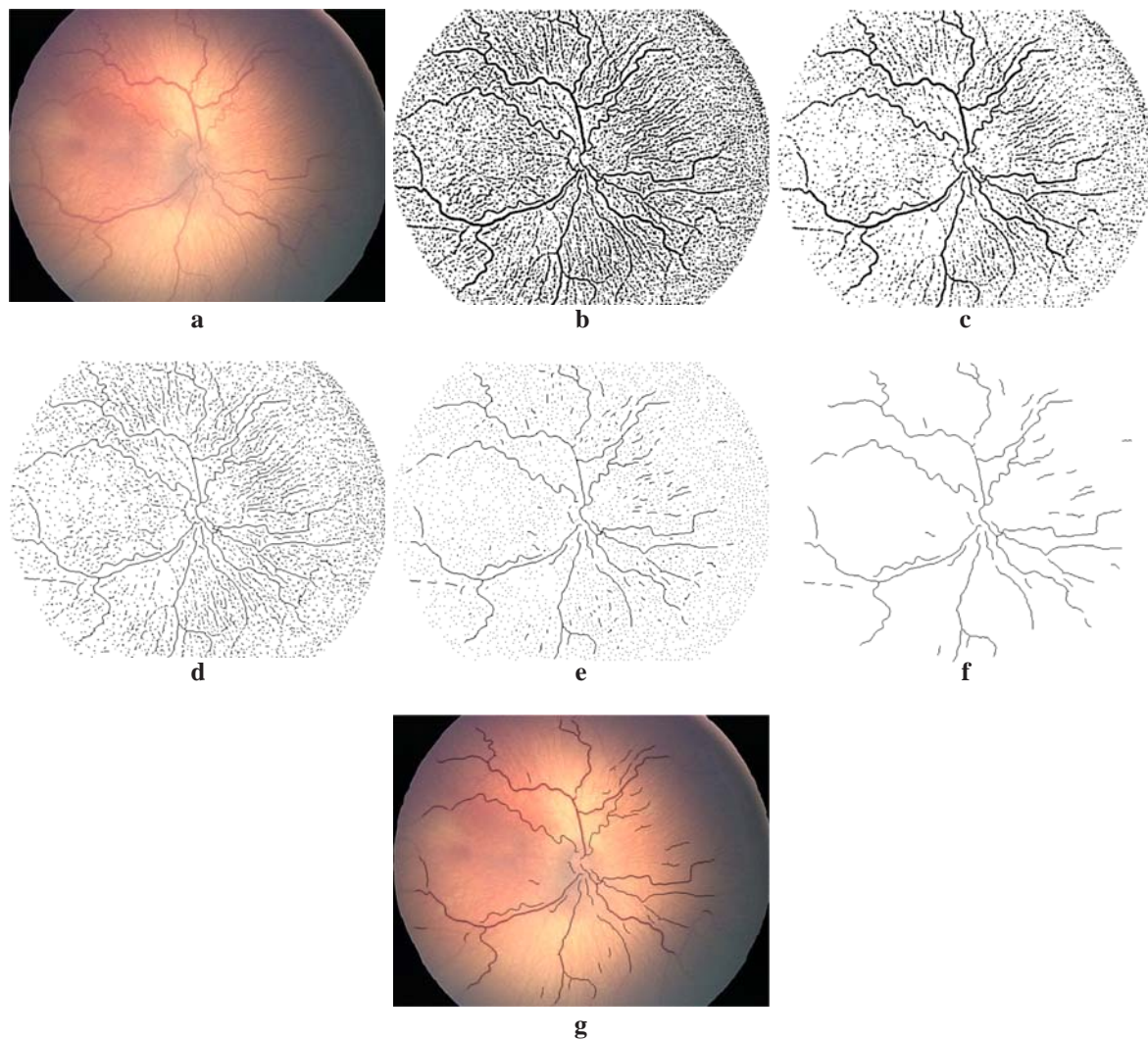
Fig. 8 (a) An original infant retinal images
(b) edge detection result
(c) after Otsu thresholding
(d) after Medial axis skeletonization
(e) after image Pruning
(f) spur removal
(g) skeletonized image super-imposed on the original

The algorithm has been tested on 100 premature infant's images with the image size of 480*640 pixels. All the results are shown in Table 1. Fig. 13 and 14 show the plot of sensitivity and specificity respectively. Fig. 15 is a plot of relationship of sensitivity and specificity for all 100 images.

Experimental results show that the proposed method performs well in extracting blood vessels.

Conclusion

In the presented paper, the authors have introduced an efficient combination of algorithms for automated blood vessel detection in infant retinal images. The proposed method retains the computational simplicity while it can achieve accurate results in cases of normal infant retinal images and images with obscured blood vessel appearance. Efficiency of the
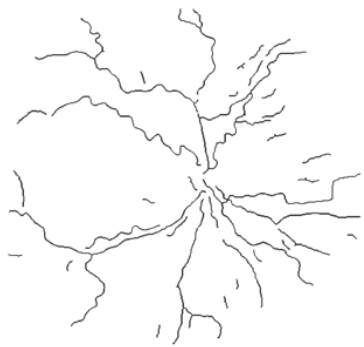
Fig. 9 Shows examples of images in each test group

a　　　　　　　　　b　　　　　　　　　c

d　　　　　　　　　e　　　　　　　　　f

Fig. 10 After the series of step are applied to (a), (b) and (c), resulting images (d), (e) and (f) are obtained respectively

a　　　　　　　　　b　　　　　　　　　c

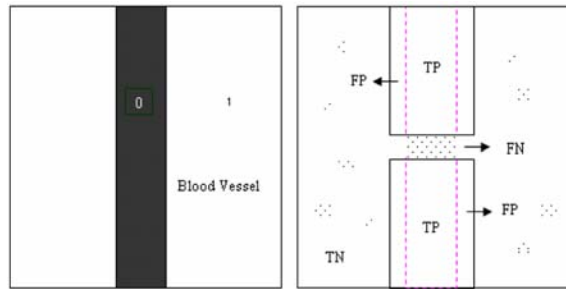**Fig. 11** (a), (b), (c) Skeletonized hand labeled ground-truth images

Fig. 12 Graphical demonstration of the calculation when
(a) is an extraction of a ground-truth image
(b) is a resulting image overlaying the ground-truth
(dash line) and resulting values

method is measured and resulted in a high specificity
of 0.9879 and sensitivity of 0.8935. The next step in this
project is to employ this approach to support tortu-
ous-based classification of ROP disease.

References
1. Retinopathy of prematurity: guidelines for screen-
   ing and treatment. The report of a Joint Working
   Party of The Royal College of Ophthalmologists
   and the British Association of Perinatal Medicine.
   Early Hum Dev 1996; 46: 239-58.
2. Heneghan C, Flynn J, O'Keefe M, Cahill M. Char-
   acterization of changes in blood vessel width and
   tortuosity in retinopathy of prematurity using im-
   age analysis. Med Image Anal 2002; 6: 407-29.
3. Swanson C, Cocker KD, Parker KH, Moseley MJ,
   Fielder AR. Semiautomated computer analysis of
   vessel growth in preterm infants without and with
   ROP. Br J Ophthalmol 2003; 87: 1474-7.
4. Wallace DK, Kylstra JA, Chesnutt DA. Prognos-
   tic significance of vascular dilation and tortuosity
   insufficient for plus disease in retinopathy of pre-
   maturity. J AAPOS 2000; 4: 224-9.
5. Kylstra JA, Freedman SF, Capowsky JJ, Hall JG.
   Measurement of retinal vessel tortuousity as a

Table 1. Sensitivity and specificity result of 100 images

Images	Group A		Group B		Group C		Group D		Group E	
	Fairly Clear Vessel		Difficult to Distinguish		Very Convoluted		Less Convoluted		Very Noisy	
	Se	Sp	Se	Sp	Se	Sp	Se	Sp	Se	Sp
1	0.860	0.988	0.881	0.989	0.936	0.978	0.923	0.980	0.830	0.994
2	0.973	0.980	0.883	0.994	0.918	0.988	0.894	0.988	0.918	0.992
3	0.898	0.990	0.863	0.996	0.842	0.976	0.912	0.988	0.898	0.996
4	0.945	0.986	0.968	0.973	0.948	0.986	0.928	0.977	0.810	0.989
5	0.971	0.973	0.942	0.981	0.955	0.973	0.935	0.989	0.850	0.997
6	0.867	0.977	0.917	0.984	0.949	0.982	0.821	0.987	0.866	0.995
7	0.916	0.979	0.900	0.972	0.993	0.982	0.882	0.986	0.647	0.997
8	0.956	0.976	0.856	0.991	0.920	0.981	0.811	0.991	0.834	0.996
9	0.950	0.972	0.895	0.990	0.935	0.986	0.909	0.988	0.728	0.996
10	0.964	0.987	0.902	0.984	0.919	0.979	0.839	0.994	0.935	0.998
11	0.944	0.983	0.842	0.983	0.895	0.973	0.879	0.996	0.835	0.984
12	0.964	0.977	0.949	0.985	0.926	0.979	0.853	0.997	0.898	0.978
13	0.977	0.985	0.944	0.980	0.919	0.977	0.943	0.979	0.743	0.990
14	0.880	0.987	0.793	0.982	0.972	0.961	0.847	0.986	0.908	0.975
15	0.912	0.987	0.929	0.986	0.939	0.984	0.910	0.986	0.884	0.993
16	0.923	0.990	0.825	0.984	0.987	0.963	0.957	0.982	0.872	0.987
17	0.837	0.990	0.915	0.992	0.940	0.967	0.957	0.982	0.805	0.989
18	0.893	0.979	0.832	0.980	0.950	0.976	0.957	0.982	0.876	0.988
19	0.902	0.977	0.815	0.998	0.920	0.983	0.964	0.985	0.948	0.981
20	0.953	0.979	0.884	0.981	0.940	0.976	0.967	0.979	0.902	0.991
Average	0.924	0.982	0.887	0.985	0.935	0.977	0.904	0.986	0.849	0.990

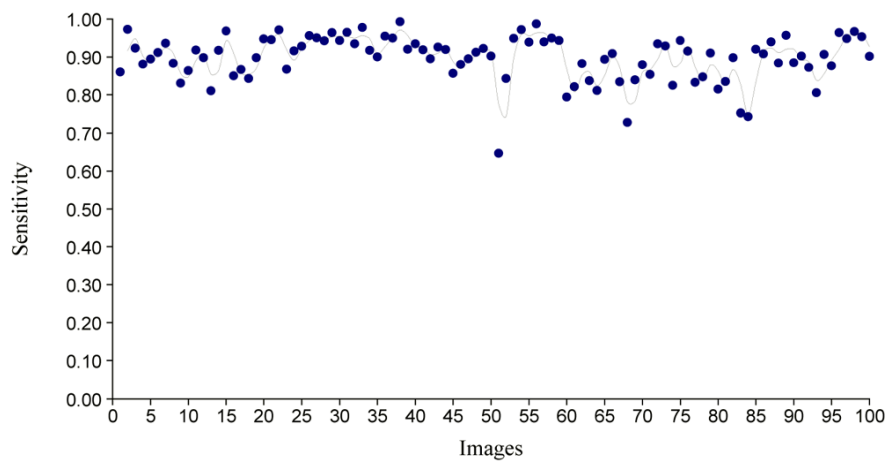Se = sensitivity
Sp = specficity

Fig. 13 A plot of sensitivity from 100 test images
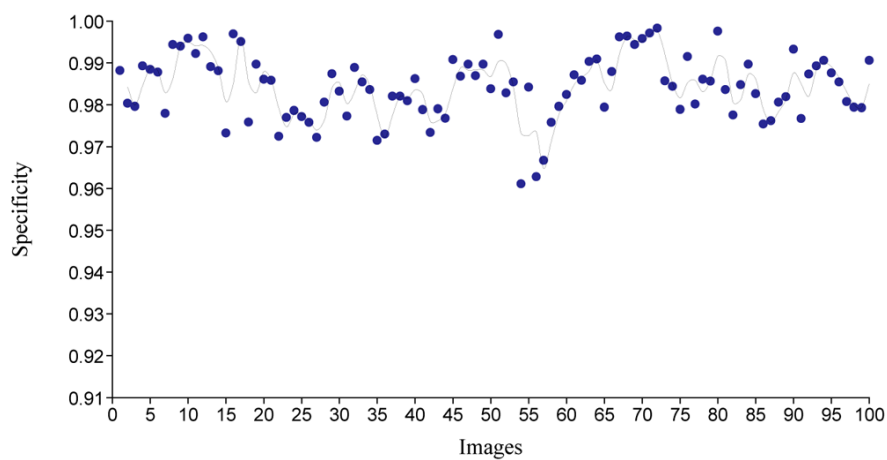

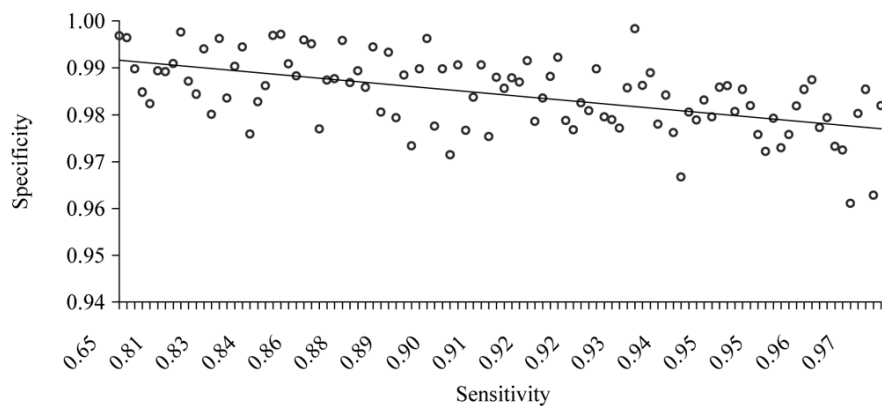
Fig. 14 A plot of specificity from 100 test images

Fig. 15 The sensitivity and specificity of segmentation (100 images)

means of diagnosis plus disease in ROP [abstract]. Invest Ophthalmol Vis Sci 1995; 36: 77.

6. Mary Ann Lang. Retinopathy of prematurity: a global problem. EnVision vol. 7, issue 1, 2002.

7. Martinez-Perez ME, Hughes AD, Stanton AV, Thom SA, Chapman N, Bharath AA, et al. Retinal vascular tree morphology: a semi-automatic quantification. IEEE Trans Biomed Eng 2002; 49: 912-7.

8. Chanwimaluang T, Fan G. An efficient algorithm for extraction of anatomical structures in retinal images. Image Processing, In Proceedings. 2003 International Conference. Barcelona, Spain; 14-17 Sept, 2003.

9. Gao XW, Bharath A, Stanton A, Hughes A, Chapman N, Thom S. Quantification and characterisation of arteries in retinal images. Comput Methods Programs Biomed 2000; 63: 133-46.

10. Canny J. A computational approach to edge detection. IEEE Trans Pattern Anal Mach Intell 1986; 8: 679-98.

11. Chaudhuri S, Chatterjee S, Katz N, Nelson M, Goldbaum M. Detection of blood vessels in retinal images using two dimensional matched filters. IEEE Trans Med Imaging 1989; 8: 263-9.

12. Byrne JPC, Ross PGB, Undrill PE, Philips RP. Feature based retinal image registration using transporter. Appl Transputer 1991; 3: 687-92.

13. Akita K, Kuga H. A computer method of understanding ocular fundus images. Pattern Recognition 1982; 15: 431-43.

14. Akita K, Kuga H. Digital processing of color ocular fundus images. in MEDINFO' 80. Amsterdam, The Netherlands: North-Holland; 1980: 80-4.

15. Akita K, Kuga H. Pattern recognition of blood vessel networks in ocular fundus images. in IEEE Int. Workshop Phys. And Eng. In Med. Imaging, Mar 15-18, 1982: 436-41.

16. Tolias YA, Panas SM. A fuzzy vessel tracking algorithm for retinal images based on fuzzy clustering. IEEE Trans Med Imaging 1998; 17: 263-73.

17. Quek FKS, Kirbas C, Gong X. Simulated wave propagation and traceback in vascular extraction. Accepted, Medical Imaging and Augmented Reality 2001 Conference, Also as VISLab Report: VISLa-01-05.

18. Hoover A, Kouznetsova V, Goldbaum M. Locating blood vessels in retinal images by piece-wise threshold probing of a matched filter response. Proc AMIA Symp 1998; 931-5.

19. Chutatape O, Zheng L, Krishnan SM. Retinal blood vessel detection and tracking by matched Gaussian and Kalman Filters. Proceeding of the 20th Annual International Conference of the IEEE Engineering in Medicine and Biology Society. 1998.

20. Zhou L, Rzeszotarski MS, Singerman LJ, Chokreff JM. The detection and quantification of retinopathy using digital angiograms. IEEE Trans on Med Img 1994; 13: 619-26.

21. Gang L, Chutatape O, Krishnan SM. Detection and measurement of retinal vessels in fundus image using amplitude modified second-order Gaussian filter. IEEE Transaction on Viomedical Engineering, Vol. 49, No. 2, February 2002.

22. Aylward S, Bullitt E. Initialization, noise, singularities, and scale in height-ridge traversal for tubular object centerline extraction. IEEE Transactions on Medical Imaging 2002: 61-75.

23. Wood SL, Qu G, Roloff LW. Detection and labeling of retinal vessels for longitidunal studies. In IEEE int Conf on Image Processing 1995; 3: 164-7.

24. Sinthanayothin C, Boyce JF, Cook HL, Williamson TH. Automated localisation of the optic disc, fovea, and retinal blood vessels from digital colour fundus images. Br J Ophthalmol 1999; 83: 902-10.

25. Nekovei R, Sun Y. Back-propagation network and its configuration for blood vessel detection in angiograms. IEEE Trans. on Neural Nets 1995; 6: 64-72.

26. Leandro JJG, Cesar RM Jr, Jeline HF. Blood vessels segmentation in retina. Preliminary Assessment of the Mathematical Morphology and of the Wavelet Transform Technique SIBGRAPI 2001, XIV Brazilian Symposium on Computer Graphics and Image processing, 15-18 October 2001, Florianpolis, Brazil.

27. Staal JJ, Kalitzin SN, Abramoff MD, Berendschot T, van Ginneken B, Viergever MA. Classifying convex sets for vessel detection in retinal images. Proceedings of the IEEE International Symposium on Biomedical Imaging. 2002: 269-72.

28. Parvin BA, Penf C, Johnston W, Maestre FM. Tracking of tubular objects for scientific applications. in Proc of the IEEE Conf on CVPR. 1994: 297-301.

29. Huang Q, Stockman GC. Generalized tube model: recognizing 3d elongated objects from 2d intensity images. in Proc of the IEEE Conf on CVPR. 1993: 104-9.

30. Aylward S, Pizer S, Bullitt E, Eberl D. Intensity ridge and widths for tabular object segmentation and registration. in Wksp on Math Methods in Biomed Image Analysis. 1996: 131-8.

31. Mahadevan V, Narasimha-Iyer H, Roysam B,

Tanenbaum HL. Robust model-based vasculature detection in noisy biomedical images. IEEE Trans Inf Technol Biomed 2004; 8: 360-76.

32. Gao XW, Bharath A, Stanton A, Hughes A, Chapman N, Thom S. Quantification and characterisation of arteries in retinal images. Comput Methods Programs Biomed 2000; 63: 133-46.

33. Vermeer KA, Vos FM, Lemij HG, Vossepoel AM. A model based method for retinal blood vessel detection. Comput Biol Med 2004; 34: 209-19.

34. Ayala G, Leon T, Zapater V. Different averages of a fuzzy set with an application to vessel segmentation. IEEE Transactions of Fuzzy Systems, Vol. 13, No. 3, June 2005.

35. Sukkaew L, Uyyanonvara B, Barman SA, Jareanjit J. Automated vessels detection on infant retinal images. accepted by 2004 International Conference on Control, Automation and Systems (ICCAS2004), August 25-27, Bangkok, Thailand: 321-5.

36. Sukkaew L, Uyyanonvara B, Barman S. Comparison of edge detection techniques on vessel detection of infant's retinal image. Proceeding of ICIM2005, October 29-30 2005, ABAC University, Bangkok, Thailand: 6.1-6.5.

37. Wallace DK, Kylstra JA, Chesnutt DA. Prognostic significance of vascular dilation and tortuosity insufficient for plus disease in retinopathy of prematurity. J AAPOS 2000; 4: 224-9.

38. Otsu N. A Threshold Selection Method from Gray-Level Histograms IEEE Transaction on Systems, Man and Cybernetics 1979;9 (1): 62-6.

39. Otsu N. A threshold selection method from gray-level histograms. IEEE Transactions on Systems, Man and Cybernetics 1979; 9: 62-6.

40. Haralick RM, Shapiro LG. Computer and robot vision. Vol. I. New York: Addison-Wesley Publishing;1992: 233, 348-49.

41. Gonzalez RC, Woods RE. Digital image processing. New York: Addison-Wesley Publishing; 1993: 540-3.

เทคนิคการตรวจหาตำแหน่งโครงสร้างเส้นเลือดอัตโนมัติในดวงตาทารกที่คลอดก่อนกำหนด

ลัสดา สุขแก้ว, บุญญฤทธิ์ อุยยานนวาระ, ซาร่า บาร์แมน, เอลสแตร์ ฟิลเดอร์, เคน ค๊อกเก้อร์

วัตถุประสงค์: เพื่อพัฒนาอัลกอริทึมในการตรวจหาโครงสร้างเส้นเลือดอัตโนมัติ บนจอประสาทตาในดวงตาทารกที่คลอดก่อนกำหนด เพื่อนำมาช่วยวิเคราะห์ปริมาณโครงข่ายการเจริญเติบโตและความผิดปกติของเส้นเลือดในดวงตาทารก retinopathy of prematurity (ROP)

วัสดุและวิธีการ: บทความฉบับนี้นำเสนอวิธีการในการตรวจหาโครงสร้างของเส้นเลือดในดวงตาทารก ซึ่งปกติจะเป็นภาพที่มีคุณภาพต่ำ มีสัญญาณรบกวนสูง เนื่องจากจะต้องถ่ายรูปภายใต้ปริมาณความเข้มแสงที่ต่ำ ระบบจะทำการวิเคราะห์ทางสถิติและเทคนิคการประมวลผลภาพ เพื่อหาค่าความเหมาะสมในการตรวจหาเส้นเลือดที่มีขนาดเล็กและบางในดวงตาทารก ซึ่งประกอบไปด้วยเทคนิคการหาขอบภาพ ด้วยตัวดำเนินการลาปาเซียนออฟเกาส์เซียนฟิลเตอร์, การแปลงภาพให้มีค่าความเข้มสองระดับโดยกำหนดค่าเทรสโฮลด์จากฮิสโตรแกรมของรูปภาพ, กระบวนการลดความกว้างของเส้นเลือดให้บางด้วยวิธีการคำนวณหาแกนกลางเส้นเลือด, การกำจัดสัญญาณรบกวนที่เป็นกลุ่มก้อนขนาดเล็กด้วยเทคนิคการทำพรุนนิ่ง

ผลการศึกษา: อัลกอริทึมที่ได้สามารถตรวจหาโครงสร้างเส้นเลือดบนภาพที่มีคุณภาพต่ำ สัญญาณรบกวนสูงและมีความชัดเจนน้อยได้ดี โดยเฉพาะตำแหน่งสำคัญที่ใช้ในการวิเคราะห์โรค ROP ซึ่งอยู่ในบริเวณขอบด้านข้างของเรตินา

สรุป: ในการทดลองได้เปรียบเทียบผลการตรวจหาโครงสร้างเส้นเลือดที่ผ่านอัลกอริทึม กับภาพวาดด้วยมือจากจักษุแพทย์ผู้เชี่ยวชาญพบว่า ผลที่ได้ให้ค่าความถูกต้องอยู่ในระดับสูง โดยให้ค่า specificity ที่ 0.9879 และค่า sensitivity ที่ 0.8935